IMAGING

Organic electronics for high-resolution electrocorticography of the human brain

Dion Khodagholy,[1]* Jennifer N. Gelinas,[1]* Zifang Zhao,[1,2]* Malcolm Yeh,[3] Michael Long,[1] Jeremy D. Greenlee,[4] Werner Doyle,[5] Orrin Devinsky,[6] György Buzsáki[1]†

Localizing neuronal patterns that generate pathological brain signals may assist with tissue resection and intervention strategies in patients with neurological diseases. Precise localization requires high spatiotemporal recording from populations of neurons while minimizing invasiveness and adverse events. We describe a large-scale, high-density, organic material–based, conformable neural interface device ("NeuroGrid") capable of simultaneously recording local field potentials (LFPs) and action potentials from the cortical surface. We demonstrate the feasibility and safety of intraoperative recording with NeuroGrids in anesthetized and awake subjects. Highly localized and propagating physiological and pathological LFP patterns were recorded, and correlated neural firing provided evidence about their local generation. Application of NeuroGrids to brain disorders, such as epilepsy, may improve diagnostic precision and therapeutic outcomes while reducing complications associated with invasive electrodes conventionally used to acquire high-resolution and spiking data.

INTRODUCTION

Electrophysiological signals recorded from the human brain provide information critical to diagnose and treat neurological diseases, as well as offering insight into cognitive processes (*1*, *2*). The brain coordinates neuronal activity across multiple spatial and temporal scales, making acquisition and interpretation of these signals challenging (*3*). Neurons communicate via action potentials or spikes, which can be recorded by placing a sensor in close proximity to the neuron, or in some cases individual axons. The aggregate synaptic and spiking activity of neurons [local field potential (LFP)] can be recorded with more distant sensors but with decreasing spatial resolution as distance increases (*4*). Placement of sensors in human subjects must minimize potential adverse effects, such as local tissue damage, hemorrhage, infection, and inflammation.

An optimal neural interface device to acquire electrophysiological signals from the human brain would be minimally invasive yet capable of precisely localizing relevant physiological or pathological activity. Although recording large-scale signals from the scalp [electroencephalography (EEG)] is often sufficient to guide clinical practice, some patients with treatment-resistant focal epilepsy require higher spatial resolution diagnostics to guide surgical resection of epileptic tissue (*5*). These patients undergo neurosurgery to record activity from electrodes placed on the cortical surface [electrocorticography (ECoG)] (*6*) or inserted into brain tissue [stereotactic depth electrodes (*7*)].

Current clinical devices for this purpose use subdurally placed electrodes that are approximately 0.5 to 5 mm in diameter and spaced 5 to 10 mm apart (*6*, *8*, *9*). Design specifications are based on historical technological limitations rather than physiologically determined resolution for detecting epileptiform activity or mapping functional regions and networks. Recordings with tissue-penetrating electrode arrays (40-μm diameter, 0.4- to 1-mm spacing) demonstrated that epileptiform activity, including high-frequency oscillations (*10*, *11*) and microseizures (*12*), can be localized with submillimeter anatomical precision. Further, the ability to record neural spiking in concert with LFP has clarified the propagation of seizure activity across the cortex (*13*) and implied more precise margins for the seizure onset zone (*14*). Despite their clinical benefits, these invasive electrodes can damage tissue and are often restricted to regions in which resection is planned, limiting their value in critical functions such as defining the border of the epileptic focus and mapping of functional areas such as language or motor cortex (*15*).

High-resolution ECoG arrays have been successfully used in large animal models to examine LFP from various cortical areas (*16*, *17*). However, barriers exist in translating these arrays to human use. Technologies based on microelectromechanical system fabrication techniques allow scaling of electrodes to cover larger surfaces, but the substrates currently used are not biocompatible or conformable (*18*). To date, none of these arrays are capable of recording neural spiking activity, due to the relatively large size and low density of the recording sites.

NeuroGrids, composed of conducting polymer [poly(3,4-ethylenedioxythiophene)/poly(styrenesulfonate) (PEDOT/PSS)] electrodes patterned at neuron-size density into an ultrathin (4 μm) parylene structure, allow acquisition of both high–spatial resolution LFP and neural spiking activity from the cortical surface (*19*). Such arrays can overcome the limitations of current neural interface devices because NeuroGrids do not penetrate or disrupt underlying brain tissue, parylene is a biocompatible substrate commonly used for long-term implantation in the human body, and the microfabrication process can be scaled to cover larger surface areas. We designed and characterized NeuroGrids specifically for human use and investigated their recording properties in subjects undergoing epilepsy surgery.

RESULTS

Our first instantiation of the NeuroGrid had a spatial coverage of ~1 mm^2 to allow investigation of cortical microcircuitry in small rodent preparations (*19*–*21*). To cover a larger spatial area with the goal

[1]NYU Neuroscience Institute, School of Medicine, New York University, New York, NY 10016, USA. [2]Neuroscience Research Institute, Peking University, Xueyuan Road, Haidian District, Beijing 10083, China. [3]Department of Neurology, University of Iowa Hospitals and Clinics, Iowa City, IA 52242, USA. [4]Department of Neurosurgery, Human Brain Research Laboratory, University of Iowa Hospitals and Clinics, Iowa City, IA 52242, USA. [5]Department of Neurosurgery, New York University Langone Medical Center, New York, NY 10016, USA. [6]Department of Neurology, Comprehensive Epilepsy Center, New York University, New York, NY 10016, USA.
*These authors contributed equally to this work.
†Corresponding author. Email: gyorgy.buzsaki@nyumc.org

of monitoring the onset and propagation of physiological (*22*, *23*) and pathological (*10*) activity patterns in the human brain, we designed NeuroGrids with either 120 or 240 electrodes to cover 420 or 840 mm^2 of neocortex, respectively (Fig. 1A). We developed a patterned "tetrode" configuration of electrodes to maintain the ability of the NeuroGrid to record spikes from neurons comprising cortical microcircuits over this larger cortical area without exceeding the number of electrodes capable of being recorded by current electrophysiological acquisition systems. Four electrodes, each sized 10 μm^2, were arranged into tetrodes with 23-μm interelectrode spacing. These tetrodes were evenly distributed at 2-mm intervals across the array (Fig. 1, B and C). This design permitted simultaneous recording of LFP at a relevant scale and detection of neural firing from neurons on adjacent electrodes within tetrodes. In addition, we added a strip of parylene on one edge of the array to allow damage-free gripping with standard surgical forceps and ease of placement on the cortical surface by the neurosurgeon.

Cerebrospinal fluid (CSF) circulation across the cortical surface is important for brain homeostatic and metabolic processes. However, the existence of substantial and/or changing amounts of fluid between the cortical surface and an electrode array causes recording instability and difficulty in recording high-frequency activity. To address this issue, we incorporated small (20 μm × 20 μm), regularly spaced physical perforations into the structure of the parylene (Fig. 1B) to facilitate extrusion and circulation of CSF after placement of the array onto the cortical surface. This design element also ensured close conformation of the entire array to the curvilinear cortical surface with minimal wrinkling and substantially decreased movement of the array relative to the cortex during normal brain pulsations. Because these small perforations were microfabricated into the structure of the NeuroGrid, they did not decrease the mechanical stability of the device.

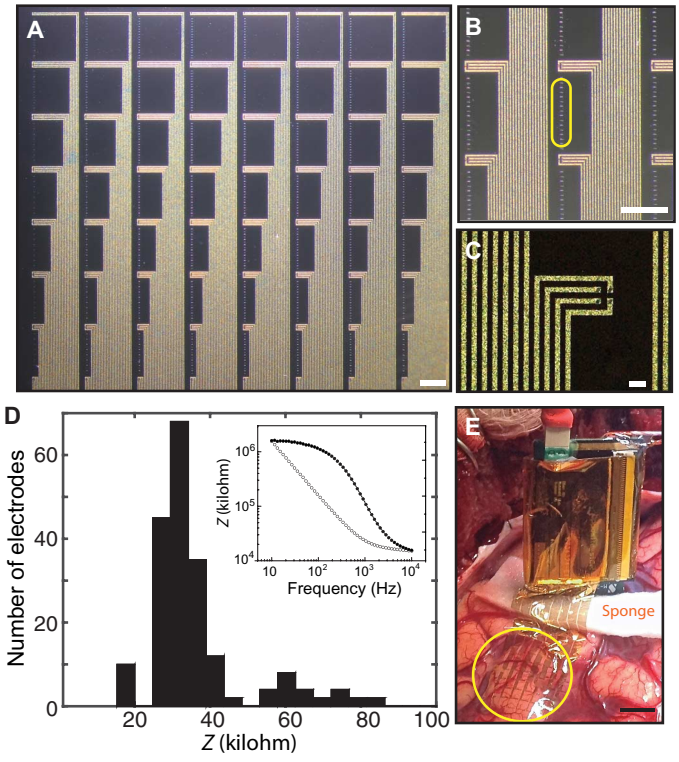

Fig. 1. NeuroGrid structure and characterization for intraoperative recording in human subjects. (**A**) Photomicrograph of 240-channel NeuroGrid. Scale bar, 1 mm. (**B**) Magnified microscopy image of 10-μm^2 electrodes arranged in 2 x 2 tetrodes, with 2-mm spacing between each tetrode. Physical perforations between electrode groups are also visible (yellow circle). Scale bar, 1 mm. (**C**) High-density patterning of conducting polymer–coated electrodes (10-μm^2 surface area, 23-μm interelectrode spacing) comprising a single tetrode. Scale bar, 20 μm. (**D**) Histogram demonstrating impedance of 240 electrodes comprising a single NeuroGrid; yield = 87.5% (210 of 240 electrodes with impedance magnitude between 10 and 100 kilohm). Inset: representative electrochemical impedance magnitude and phase of a single electrode across the range of physiological frequencies. (**E**) Intraoperative photograph showing 240-channel NeuroGrid (yellow circle) conforming to the surface of the cortex with accompanying headstage. Scale bar, 1 cm.

The yield of functional electrodes (impedance, 10 to 100 kilohm) within a single NeuroGrid was consistently high (80 to 100%; Fig. 1D). Impedance was maintained over the range of physiological frequencies (Fig. 1D, inset). Arrays were sterilized for intraoperative use with a conventional gas sterilization protocol, and electrode impedance measurements were not altered between pre- and poststerilization. The backend of the array was connected to a custom-made headstage (18 mm × 26 mm × 0.6 mm) via a zero insertion force (ZIF) connector, and data (sampled at 20 kHz) were transmitted to the amplifier via a thin, flexible cable capable of transmitting data from a maximum of 128 channels. Therefore, data acquisition was performed using either one (for 120-electrode NeuroGrids) or two (for 240-electrode NeuroGrids) headstages, each attached to one cable. This recording setup allowed the neurosurgeon to suspend the headstage above the brain surface with a flexible LEYLA arm, making it possible to accommodate recording from various sizes and orientations of craniotomies (Fig. 1E). Placement of the array was dictated by the clinically indicated position of the craniotomy and was always adjacent to the suspected seizure onset zone.

We successfully acquired LFP and action potentials with NeuroGrids from five human neurosurgery subjects (table S1). Subjects were undergoing surgery with different general anesthetic regimes (n = 4) or awake craniotomy for functional language mapping (n = 1). First, we examined large-scale brain state–dependent dynamics and found that LFP recorded with NeuroGrids matched known activity patterns induced by anesthetic agents (*24*). In one subject, propofol generated a burst suppression pattern characterized by periods of relative isoelectric activity alternating with periods of δ (1 to 4 Hz) and α (8 to 12 Hz) band frequency oscillations, visible both in the raw LFP trace and on associated spectrograms (Fig. 2A). In contrast, a subject under sevoflurane anesthesia exhibited prominent, relatively continuous sequences of δ, α, and β (10 to 20 Hz) band frequency oscillations (Fig. 2B). For the awake subject, we recorded with a NeuroGrid in parallel with two conventional strip electrodes connected to clinical video EEG monitoring equipment. In this brain state, both recordings demonstrated an α peak (~10 Hz) typical for awake subjects (Fig. 2, C and D) (*24*). In addition, multiple interictal epileptiform discharges (IEDs) were identified by both the NeuroGrid and clinical strips, visible as sharp transients on the raw LFP traces or spectrograms. NeuroGrid recordings contained proportionately more γ band (>40 Hz) power than the clinical recordings, potentially attributable to differences in electrode geometry and location. These data established the ability of the neuron scale (10 μm^2) NeuroGrid electrodes to capture and compare brain state dynamics conventionally recorded with much larger electrodes (approximately 12 mm^2).

Next, we investigated LFP activity at higher spatiotemporal resolution. During sevoflurane anesthesia, epochs (300 to 3000 ms) of β band frequency were prominent. We detected these epochs in the

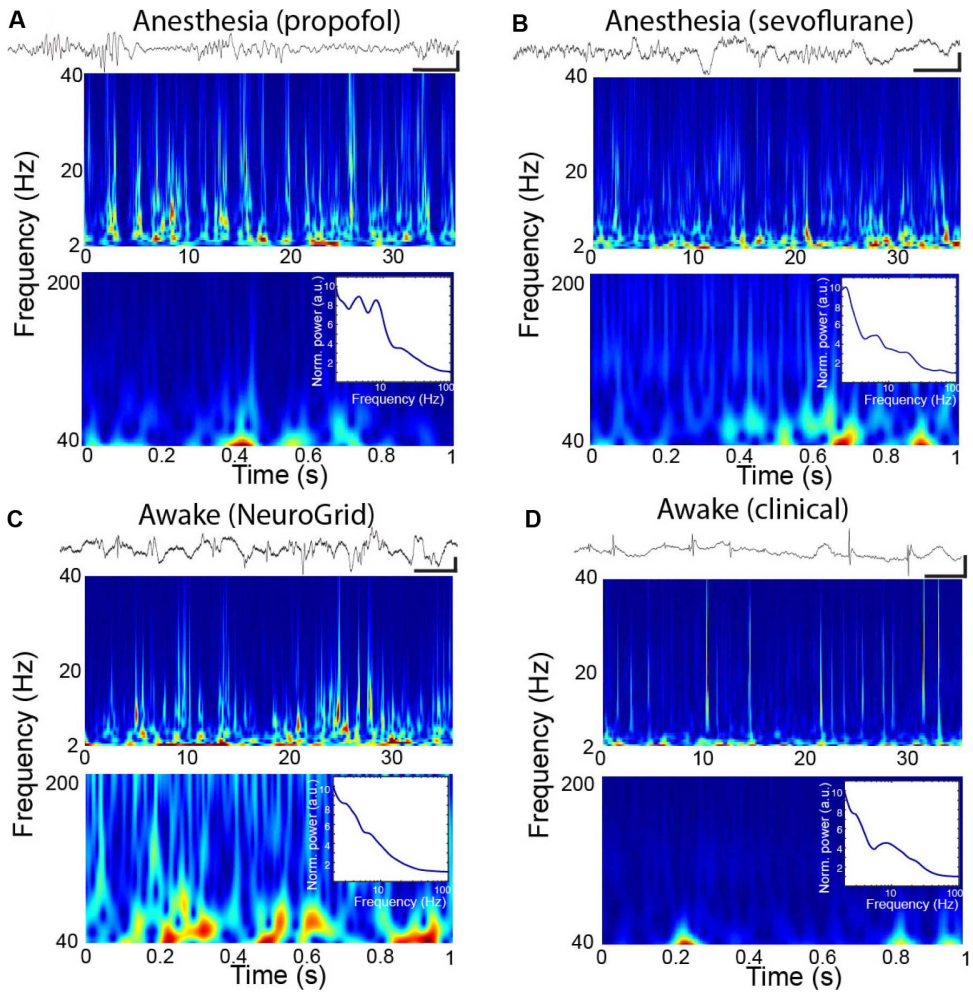

Fig. 2. Intraoperative NeuroGrid recordings reveal brain state dynamics in anesthetized and awake human subjects. (**A**) Raw LFP trace (top) and corresponding low- (middle) and high-frequency (bottom) spectrograms from a subject under propofol anesthesia using a 120-electrode NeuroGrid; corresponding power spectrum shown as an inset. Scale bar, 500 ms, 200 μV. a.u., arbitrary units. (**B**) Subject under low-concentration sevoflurane anesthesia using a 240-electrode NeuroGrid; conventions as in (A). Scale bar, 500 ms, 200 μV. (**C**) NeuroGrid recording from awake subject participating in language mapping tasks using a 120-electrode NeuroGrid; conventions as in (A). Scale bar, 1 s, 500 μV. (**D**) Clinical ECoG recording from awake subject in (C) participating in language mapping tasks; conventions as in (A). Scale bar, 1 s, 500 μV.

raw LFP and trigger-averaged β band frequency power across the array, revealing spatially coherent clustering of activity (Fig. 3A). We also analyzed IEDs recorded by the NeuroGrid during awake craniotomy. Visualization of the raw IED waveform and its peak amplitude measurement across the spatial extent of the NeuroGrid revealed a fine-scale patterning of activity with a restricted spatial distribution. Furthermore, IED waveforms were not synchronous across the array, and latency analysis demonstrated a progressive delay suggestive of IED propagation (Fig. 3B).

In addition to fine-scale LFP acquisition, NeuroGrids can record spiking activity from the cortical surface. High-pass–filtered (250 Hz) traces from individual electrodes yielded spiking activity in both anesthetized and awake subjects (Fig. 3C), although spontaneous firing rates were higher in the awake subject as expected. Because of the tetrode configuration of electrodes on our array, we could also record action potential waveforms of individual neurons (spikes) on adjacent electrodes. Spike waveforms displayed maximal peak negativity at the detection electrode, with a decrement in amplitude or polarity reversal on adjacent recording sites of the local tetrode (Fig. 3D), reflecting micrometer-scale sources and sinks in the extracellular space. A key advantage of the tetrode configuration is that action potential waveforms could be attributed to different neurons based on their differential spatial pattern across the electrodes of the tetrode (Fig. 3D, bottom left tetrode).

Furthermore, we examined the relationship between LFP and spiking activity in anesthetized and awake subjects. Under anesthesia, neurons significantly decreased their firing rate at the trough of local δ waves ("down" state; Fig. 3E), and a subset of neurons displayed robust phase-locking to β frequency oscillations (Fig. 3F). The location of these neurons corresponded to zones of maximal β frequency power in the LFP. IEDs during waking were associated with decreased firing of a subset of neurons over a restricted anatomical area after the time of the local peak negativity of the IED waveform and corresponding to the post-spike slow wave (Fig. 3G). We did not observe a robust increase in firing rate during the time of IED waveform, potentially indicating that the NeuroGrid was outside of the seizure onset zone, where neurons are largely inhibited (*13*). Together, these analyses demonstrate that NeuroGrid recordings can simultaneously

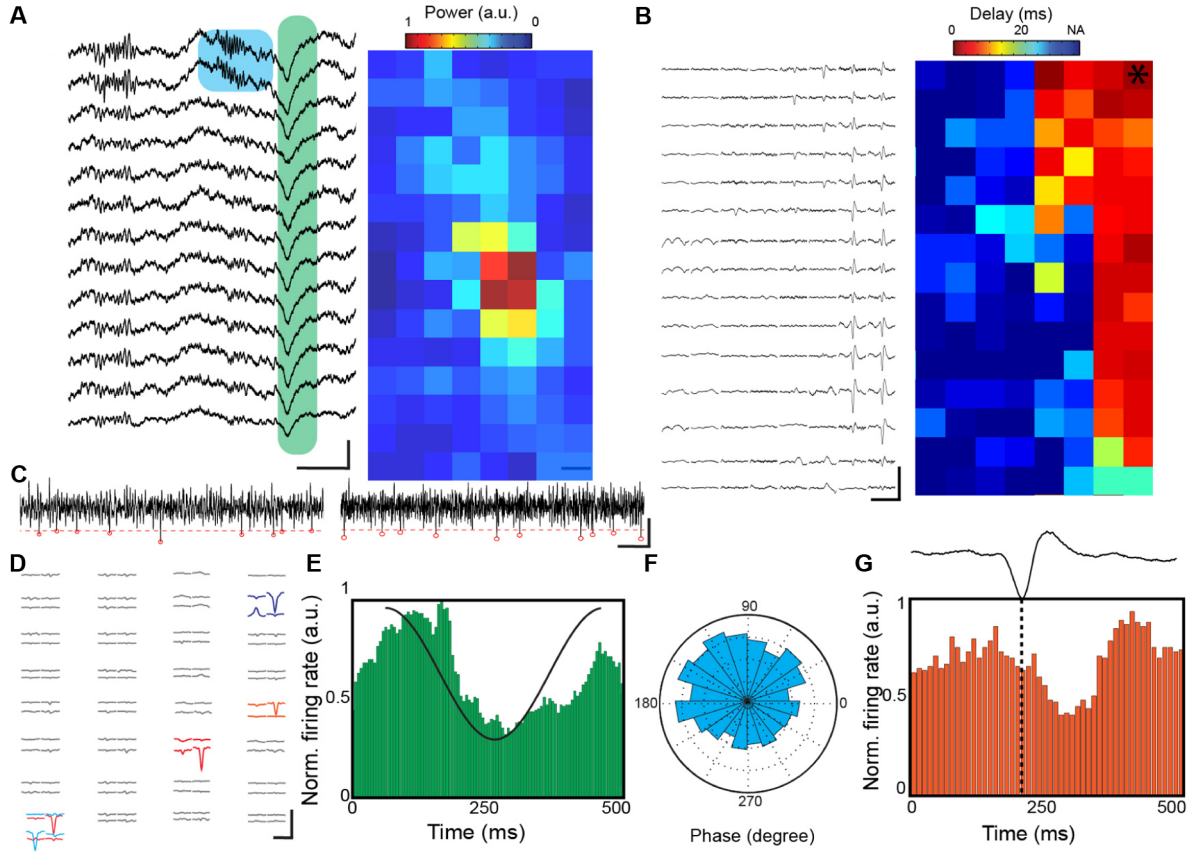

Fig. 3. Spatial distribution of localized LFP and neural spiking activity across the NeuroGrid. (**A**) Raw LFP traces (left) from multiple recording electrodes of the NeuroGrid in a subject under general anesthesia using a 120-electrode NeuroGrid demonstrating localized β frequency oscillation (blue) and δ wave (green). Scale bar, 500 ms, 200 μV. Corresponding colormap of power in β frequency band across 8 × 15 array. (**B**) Raw LFP traces (left) from electrodes across the NeuroGrid in an awake subject using a 120-electrode NeuroGrid reveal localized distribution of IED waveform. Scale bar, 0.5 s, 1 mV. Corresponding colormap of latency to maximal negativity of IED waveform; * denotes reference electrode for latency measurement; electrodes that do not exhibit an IED waveform are in dark blue. (**C**) High-pass–filtered traces (250 Hz) from subject in (B) during the listening phase of a language task (left) and from subject under anesthesia using a 240-electrode NeuroGrid (right). Red dashed line shows 3× noise floor; red circles are peaks of detected action potentials. Scale bar, 25 ms, 60 μV. (**D**) Examples of the spatial extent of extracellular action potentials over the geometry of the array by spike-triggered averaging during the detected spike times from subject in (B). Scale bar, 1.5 ms, 50 μV. (**E**) Average normalized neural firing rate recorded from representative electrode during δ wave (average waveform overlaid in black) from subject under sevoflurane anesthesia using 240-electrode NeuroGrid. (**F**) Polar plot showing phase-locking of sample neural firing to β frequency oscillations recorded from representative electrode during sevoflurane anesthesia using a 120-electrode NeuroGrid. (**G**) Sample average normalized neural firing rate during time window of IED occurrence in awake subject. Black trace (top) is average IED waveform, with dashed line denoting time of the local peak negativity of the IED waveform.

provide information about large-scale brain state, generation and propagation of focal LFP patterns, and spiking activity of neurons.

What spatial sampling is required to identify the anatomical distribution of various brain oscillations? Because the distances between pairs of electrodes on NeuroGrids ranged from 30 μm to 16 mm, we investigated this question by determining the coherence over distance for various frequency bands (1 to 90 Hz) in anesthetized and awake states. At mid-γ frequency (75 to 90 Hz), a band that encompasses the maximal power generated by IEDs (*9*) and is often used as a marker for local cortical processing in ECoG studies (*25*), coherence decreased precipitously within 2 mm in both states, but coherence was consistently lower during waking (Fig. 4, A and B). We conducted a similar analysis for data recorded under anesthesia with our 1-mm^2 NeuroGrid to further examine the coherence decrease within the first millimeter and observed a relatively linear decrement (Fig. 4C). As predicted by theoretical models of spatial scale of LFP (*26*), coherence was higher and decreased more slowly with decreasing frequency. On the scale of neural spiking, action potentials from an individual neuron were only visible on electrodes within 50 μm of the electrode with the maximal waveform amplitude (Fig. 3D). Overall, these analyses suggest that LFP patterns can be differentiated at submillimeter distances and that high spatiotemporal resolution sampling of neural activity can provide information about physiological and pathological cortical processes.

DISCUSSION

The NeuroGrids are capable of acquiring high spatiotemporal resolution neurophysiologic signals from the cortical surface in humans and are amenable to translation to clinical use. NeuroGrids have several advantages compared to current clinical arrays or research arrays used in large animal models, including (i) ultrathin and conformable structure, (ii) scalability and design variability, (iii) efficient preamplification and data transmission, and (iv) simultaneous acquisition of LFP and action potentials without penetrating the brain surface.

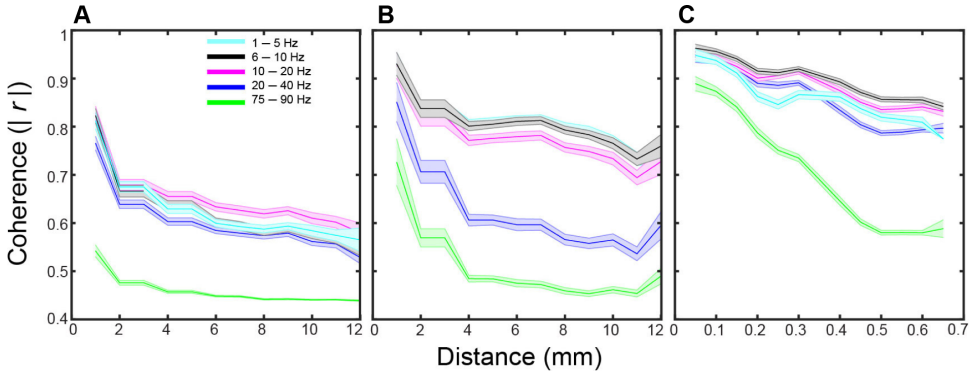

Fig. 4. Coherence of neural activity patterns at millimeter and micrometer scales in anesthetized and awake human subjects. (**A**) Coherence between recording electrodes spaced over millimeters at each frequency band in the awake subject using 120-electrode NeuroGrid. Coherence values for pairs of electrodes were averaged in bins of 2 mm and plotted as means ± SEM. (**B**) Coherence between recording electrodes spaced over millimeters at each frequency band in an anesthetized subject using 120-electrode NeuroGrid. Conventions as in (A). (**C**) Coherence between recording electrodes spaced over hundreds of micrometers at each frequency band in an anesthetized subject using 64-electrode NeuroGrids. Coherence values for pairs of electrodes were averaged in bins of 100 μm and plotted as means ± SEM. Color conventions as in (A).

Increasing the size of subdural grid implants is associated with a higher incidence of adverse effects in patients (*27*). Large clinical subdural grids are more rigid and may thereby exert more direct pressure on the cortical surface and be less able to accommodate cerebral edema that occurs as a result of the grid-induced inflammation, seizures, anesthesia, or surgery (*28*). The resultant increase in intracranial pressure could restrict CSF flow or compromise arterial or venous circulation, impairing local metabolic support and clearance (*29*). Because NeuroGrids are ultrathin (4 μm thick), conformable, and lightweight, they likely exert negligible pressure on the cortical surface. Further, physical perforations in the NeuroGrid array facilitate wrinkle-free placement, allowing circulation and extrusion of CSF in case of increasing intracranial pressure. In all of our surgical cases, we recorded neurophysiological data without causing any observable effect on brain tissue, and no adverse events were reported postoperatively. Although polyimide-based arrays can be thin (20 to 30 μm), they are not conformable, and polyimide is not yet recognized as a biocompatible substrate for human use (*17*, *30*, *31*). Despite their thinness, our NeuroGrids were also robust to manipulation by the neurosurgeon with conventional instruments after a short training session.

NeuroGrids can be scaled in size and varied in geometry depending on the cortical surface area to be covered. This customization can address both anatomical requirements for different surgical procedures and the spatial scale required for different neuroscientific and clinical questions. For instance, the instantiation of the NeuroGrid discussed here is composed of grouped electrodes to permit identification of action potential waveforms from putative single neurons, essential information for microcircuit analysis. If recording of multiunit activity is sufficient, electrode positioning can be adjusted to provide uniform spacing across larger arrays. As stronger links are forged between electrophysiological patterns and epilepsy surgery outcomes, designs that acquire the most useful physiological patterns can be established. Also, NeuroGrids may provide safety and efficacy advantages to routine clinical subdural electrodes in mapping areas that serve functions such as language and motor control.

We have also addressed how to couple the conformable NeuroGrids with silicon-based technologies (rigid electronics) for data preamplification and transmission. A ZIF connector provides adequate mechanical stability and allows integration with custom-built or commercial amplifiers through a printed circuit board (PCB). Alternatively, the arrays can be directly interfaced with a PCB via ball grid array soldering techniques. However, we found that this method decreased the yield of functional NeuroGrid electrodes, possibly due to alignment issues. We minimized the physical size of these backend components to facilitate intraoperative handling but also ensured that data were multiplexed at this stage to allow transmission of data from up to 128 channels with a single thin, flexible cable. Because the size of material implanted and the number of cables traversing the subcutaneous tissue are correlated with increased infection rate (*32*), our design can simplify the translation of NeuroGrid technology to postsurgical intrahospital monitoring. Furthermore, NeuroGrids can be customized into an embedded acquisition system by routing data directly from the headstage to a miniaturized, attached data storage device (such as a microsecure digital card) or a closed-loop system by including a microcontroller for online computation.

In keeping with theoretical and experimental findings of LFP generation and its acquisition by recording electrodes (*3*, *4*, *23*, *33*–*35*), we recorded brain state–dependent patterns of activity during anesthesia and awake states with the low-impedance, small electrodes of the NeuroGrid. In low-frequency bands, NeuroGrid recordings did not differ from recorded data acquired by conventional large subdural electrodes. This result suggests that the use of high-resolution, large-scale NeuroGrids can satisfy current classical clinical diagnostics. Moreover, NeuroGrid recordings provide highly localized and high-frequency information that may improve interpretation of lower-frequency signals. For instance, determination of the anatomical focus that has the peak amplitude or earliest latency of an IED waveform with high spatial resolution could help narrow zones of onset and propagation pathways of epileptiform activity within the cortex (*36*, *37*). Comparing LFP and spiking activity on the same electrode, we demonstrated spike entrainment to the IED waveform. In the current case, we found a marked decrease of unit firing immediately after the IED. Because 30 to 50% of neurons typically increase their firing during an IED in the seizure onset zone (*38*, *39*), it is possible that we recorded outside of this zone but in a cortical area still affected by post-IED inhibition, as occurs with propagation of ictal activity (*13*). Determining spike-LFP synchrony during IEDs could identify brain regions that are actively recruited into epileptiform activity, providing a more accurate delineation of epileptogenic brain tissue for possible resection.

By recording wideband signals from electrodes spaced tens of micrometers to tens of millimeters apart, the spatial spread of LFP and spiking activity can be quantified in the human brain. The coherence between mid-γ waves (75 to 90 Hz) on separate electrodes decreased substantially and relatively linearly with distance, illustrating the ability of high–spatial resolution sampling to identify localized patterns that represent activity of small populations of neurons (*11*, *12*, *14*, *36*, *40*).

We have established the feasibility and safety of NeuroGrids to record high-quality electrophysiological signals in anesthetized and awake human subjects. The simultaneous acquisition of high–spatial resolution LFP with spiking activity may help interpret physiological and pathological patterns, without impeding identification of these patterns currently acquired by clinical arrays and amplifiers. Adaptation of NeuroGrids and associated components for prolonged recordings in patients with epilepsy will advance our capacity to define neurophysiological signatures and potentially improve the diagnostic precision of ECoG while reducing morbidity due to invasive electrodes.

MATERIALS AND METHODS

Probe fabrication and characterization

The fabrication and patterning of PEDOT/PSS-based NeuroGrids have been discussed in previous publications (*41*–*43*). A projection exposure system was used to deposit and pattern parylene C, Au, Pt, Ti, and PEDOT/PSS films. First, parylene C was deposited using an SCS Labcoter 2 to a thickness of 2 μm (to ensure pinhole-free films). We used 3-(trimethoxysilyl)propyl methacrylate (A-174 Silane) as an adhesion promoter and a dilute solution of industrial cleaner (Micro-90) as an antiadhesion agent. Next, the film was patterned with a 4.5-μm-thick layer of SPR220-45 (Electronic Materials) photoresist and dry-etched with a plasma reactive ion etching process (Oxford 80 Plus; 180 W, 50-sccm O_2, 3-sccm SF6, 2-sccm CF4 for 15 min). A lift-off process was used to pattern metal pads and interconnects. AZ nLOF 2020 (a negative photoresist) was spin-coated on the parylene film (5500 rpm), baked at 115°C for 60 s, exposed using a stepper (GCA Autostep 200 DSW i-line Wafer Stepper), and finally developed (MF726 developer). With use of an e-beam metal evaporator (CVC SC4500 at 2.10^{-6} bars), metallic layers of Ti (10 nm), Pt (150 nm), and Au (50 nm) were deposited. Lift-off was performed using 1165 stripper (2 hours).

To enhance the conductivity of PEDOT/PSS, a mixture of PEDOT/PSS aqueous dispersion (PH-1000 from H. C. Stark) and ethylene glycol (20:5 ml ratio) was prepared and mixed with dodecylbenzenesulfonic acid (100 μl per 50 ml) and 3 glycidoxypropyltrimethoxysilane (1 weight %) to adjust surface energy and cross-link, respectively. The resulting dispersion was spin-coated in two steps with soft bake in between (120°C, 60 s) at 650 rpm. The films were subsequently baked at 140°C for 1 hour and then immersed in deionized water overnight to remove any excess low–molecular weight compounds. The electrodes were characterized in vitro using phosphate-buffered saline solution. A significantly larger Ag/AgCl wire compared to electrode geometry served as the reference electrode for impedance spectroscopy and measurements.

Probe backend design and construction

The NeuroGrid was attached to a custom PCB via a ZIF connector. The board contained two or four (120 or 240 channel) RHD2164 dies (Intan Technologies) directly wire-bonded to the board for the purposes of amplification, digitization, and transmission of the acquired neural signal via a serial peripheral interface protocol to a computer interface board (RHD2000 evaluation board, Intan Technologies). The ZIF board was completely covered with medical-grade silicone elastomer for ease of handling and reduction of sharp edges.

Intraoperative human subject recordings

Intraoperative human subject recordings were approved by the Institutional Review Board (IRB) at New York University Langone Medical Center (NYULMC) or the IRB at the University of Iowa Hospitals and Clinics (UIHC). Subjects undergoing epilepsy surgery for placement of clinical subdural ECoG arrays or resection of epileptic tissue were eligible for the study. Subjects with diffuse cortical lesions, with developmental disability, or who were less than 18 years of age were excluded. Informed written consent was obtained from all subjects for all aspects of the protocol, including publication of photos. All electronic equipment used in the operating room was checked and approved by the Clinical Engineering Department at NYULMC or UIHC. NeuroGrids, headstages, and associated cables were sterilized using a conventional gas sterilization protocol (97 to 100% ethylene oxide at 50° to 60°C for 4 hours followed by 12 hours of detoxification). To prevent mechanical damage to the NeuroGrids during the sterilization procedure, devices were sutured to custom sterilization boxes and released for use only in the operating room. Recordings lasted for a maximum of 30 min and were performed either under anesthesia or during awake craniotomy as determined by the clinical protocol, attending neurosurgeon, and anesthesiologist. Four recordings were performed at NYULMC under anesthesia, and one awake craniotomy recording was performed at the UIHC. Placement of the array was guided by location of craniotomy required for clinical diagnostic and therapeutic procedures, and by advice of the attending neurosurgeon. Stainless steel reference and ground electrodes were attached adjacent to the recording area.

Characteristics of human subjects

Of our five subjects, three were female and two were male, ranging from 24 to 60 years of age. All subjects had epilepsy and were candidates for epilepsy surgery based on either refractory focal seizures or lesion-related seizures. Array placement was on the superior or middle temporal gyrus in four subjects, and inferior frontal gyrus in one subject. One subject had a lesion in the vicinity of language areas in the dominant hemisphere and thus underwent awake craniotomy for functional language mapping. For recordings performed under anesthesia, different anesthetic regimes were used (subject 1: dexmedetomidine, propofol, and remifantyl; subjects 2 and 3: sevoflurane and remifentanyl; subject 4: propofol).

Data acquisition and processing

Neurophysiological signals were amplified, digitized continuously at 20 kHz using a headstage directly attached to the NeuroGrid, and stored for offline analysis with 16-bit format. Data were analyzed using MATLAB (MathWorks) and visualized using NeuroScope (neurosuite.sourceforge.net). An amplitude threshold method was used to detect spikes from bandpass-filtered data (0.25 to 2.5 kHz). IEDs were detected as follows: (i) bandpass filtering at 25 to 80 Hz and signal rectification, (ii) detection of events where the filtered envelope was more than two times above baseline, and (iii) elimination of events where the unfiltered envelope was less than two times above baseline. Detected IEDs had waveforms consistent with typical interictal spikes and/or sharp waves. All detections were visually inspected for accuracy for each recording session.

Clinical data acquisition and processing

For the subject at UIHC, concurrently recorded clinical ECoG was available. Two conventional subdural strips (Ad-Tech Medical) were placed in proximity to the NeuroGrid, and neurophysiological signals were acquired using a Neurofax EEG system, sampled at 500 Hz, and stored for subsequent offline analysis. These data were imported into MATLAB and resampled to 1250 Hz for IED detection as described for the research array data.

Data and statistical analysis

Analysis was performed using a combination of freely available online MATLAB toolboxes (Freely Moving Animal Toolbox; http://fmatoolbox.sourceforge.net) and custom MATLAB code. Spectrograms were generated using wavelet transformation (Gabor), and coherence was calculated using multitaper time-frequency analysis (Chronux; http://chronux.org/). The instantaneous LFP phase was extracted by Hilbert transform and validated with wavelet transformation to ensure uniform phase distribution. Units were deemed to have phase-locking to LFP oscillations when $\alpha < 0.05$ and $\kappa > 0.1$ on Rayleigh's test of non-uniformity.

SUPPLEMENTARY MATERIALS

Supplementary material for this article is available at http://advances.sciencemag.org/cgi/content/full/2/11/e1601027/DC1

table S1. Yield of LFP and spike data from NeuroGrid recordings.

REFERENCES AND NOTES

1. J. Jacobs, M. J. Kahana, Direct brain recordings fuel advances in cognitive electrophysiology. *Trends Cogn. Sci.* **14**, 162–171 (2010).
2. P. Gloor, Contributions of electroencephalography and electrocorticography to the neurosurgical treatment of the epilepsies. *Adv. Neurol.* **8**, 59–105 (1975).
3. C. M. Lewis, C. A. Bosman, P. Fries, Recording of brain activity across spatial scales. *Curr. Opin. Neurobiol.* **32**, 68–77 (2015).
4. G. Buzsáki, C. A. Anastassiou, C. Koch, The origin of extracellular fields and currents—EEG, ECoG, LFP and spikes. *Nat. Rev. Neurosci.* **13**, 407–420 (2012).
5. E. Behrens, J. Zentner, D. van Roost, A. Hufnagel, C. E. Elger, J. Schramm, Subdural and depth electrodes in the presurgical evaluation of epilepsy. *Acta Neurochir.* **128**, 84–87 (1994).
6. A. R. Wyler, G. A. Ojemann, E. Lettich, A. A. Ward Jr., Subdural strip electrodes for localizing epileptogenic foci. *J. Neurosurg.* **60**, 1195–1200 (1984).
7. J. Gonzalez-Martinez, J. Mullin, S. Vadera, J. Bulacio, G. Hughes, S. Jones, R. Enatsu, I. Najm, Stereotactic placement of depth electrodes in medically intractable epilepsy. *J. Neurosurg.* **120**, 639–644 (2014).
8. N. Mesgarani, C. Cheung, K. Johnson, E. F. Chang, Phonetic feature encoding in human superior temporal gyrus. *Science* **343**, 1006–1010 (2014).
9. J. N. Gelinas, D. Khodagholy, T. Thesen, O. Devinsky, G. Buzsáki, Interictal epileptiform discharges induce hippocampal–cortical coupling in temporal lobe epilepsy. *Nat. Med.* **22**, 641–648 (2016).
10. A. Bragin, C. L. Wilson, R. J. Staba, M. Reddick, I. Fried, J. Engel Jr., Interictal high-frequency oscillations (80-500Hz) in the human epileptic brain: Entorhinal cortex. *Ann. Neurol.* **52**, 407–415 (2002).
11. A. Bragin, J. Engel Jr., C. L. Wilson, I. Fried, G. Buzsáki, High-frequency oscillations in human brain. *Hippocampus* **9**, 137–142 (1999).
12. M. Stead, M. Bower, B. H. Brinkmann, K. Lee, W. R. Marsh, F. B. Meyer, B. Litt, J. Van Gompel, G. A. Worrell, Microseizures and the spatiotemporal scales of human partial epilepsy. *Brain* **133**, 2789–2797 (2010).
13. C. A. Schevon, S. A. Weiss, G. McKhann Jr., R. R. Goodman, R. Yuste, R. G. Emerson, A. J. Trevelyan, Evidence of an inhibitory restraint of seizure activity in humans. *Nat. Commun.* **3**, 1060 (2012).
14. S. A. Weiss, G. P. Banks, G. M. McKhann Jr., R. R. Goodman, R. G. Emerson, A. J. Trevelyan, C. A. Schevon, Ictal high frequency oscillations distinguish two types of seizure territories in humans. *Brain* **136** (Pt. 12), 3796–3808 (2013).
15. A. Waziri, C. Schevon, J. Cappell, Initial surgical experience with a dense cortical microarray in epileptic patients undergoing craniotomy for subdural electrode implantation. *Neurosurgery* **64**, 540–545 (2009).
16. J. Viventi, D.-H. Kim, L. Vigeland, E. S. Frechette, J. A. Blanco, Y.-S. Kim, A. E. Avrin, V. R. Tiruvadi, S.-W. Hwang, A. C. Vanleer, D. F. Wulsin, K. Davis, C. E. Gelber, L. Palmer, J. Van der Spiegel, J. Wu, J. Xiao, Y. Huang, D. Contreras, J. A. Rogers, B. Litt, Flexible, foldable, actively multiplexed, high-density electrode array for mapping brain activity in vivo. *Nat. Neurosci.* **14**, 1599–1605 (2011).
17. B. Rubehn, C. Bosman, R. Oostenveld, P. Fries, T. Stieglitz, A MEMS-based flexible multichannel ECoG-electrode array. *J. Neural Eng.* **6**, 036003 (2009).
18. C. Hassler, T. Boretius, T. Stieglitz, Polymers for neural implants. *J. Polym. Sci. Part B Polym. Phys.* **49**, 18–33 (2011).
19. D. Khodagholy, J. N. Gelinas, T. Thesen, W. Doyle, O. Devinsky, G. G. Malliaras, G. Buzsáki, NeuroGrid: Recording action potentials from the surface of the brain. *Nat. Neurosci.* **18**, 310–315 (2015).
20. D. Khodagholy, T. Doublet, P. Quilichini, M. Gurfinkel, P. Leleux, A. Ghestem, E. Ismailova, T. Hervé, S. Sanaur, C. Bernard, G. G. Malliaras, In vivo recordings of brain activity using organic transistors. *Nat. Commun.* **4**, 1575 (2013).
21. D. Khodagholy, T. Doublet, M. Gurfinkel, P. Quilichini, E. Ismailova, P. Leleux, T. Herve, S. Sanaur, C. Bernard, G. G. Malliaras, Highly conformable conducting polymer electrodes for in vivo recordings. *Adv. Mater.* **23**, H268–H272 (2011).
22. Y. Nir, R. J. Staba, T. Andrillon, V. V. Vyazovskiy, C. Cirelli, I. Fried, G. Tononi, Regional slow waves and spindles in human sleep. *Neuron* **70**, 153–169 (2011).
23. G. Buzsáki, Large-scale recording of neuronal ensembles. *Nat. Neurosci.* **7**, 446–451 (2004).
24. P. L. Purdon, A. Sampson, K. J. Pavone, E. N. Brown, Clinical electroencephalography for anesthesiologists: Part I: Background and basic signatures. *Anesthesiology* **123**, 937–960 (2015).
25. A. M. Bastos, J. Vezoli, C. A. Bosman, J.-M. Schoffelen, R. Oostenveld, J. R. Dowdall, P. De Weerd, H. Kennedy, P. Fries, Visual areas exert feedforward and feedback influences through distinct frequency channels. *Neuron* **85**, 390–401 (2015).
26. H. Lindén, T. Tetzlaff, T. C. Potjans, K. H. Pettersen, S. Grün, M. Diesmann, G. T. Einevoll, Modeling the spatial reach of the LFP. *Neuron* **72**, 859–872 (2011).
27. Z. Rahman, A. F. Bleasel, M. Bartley, M. Dexter, T. Galea, D. Gill, S. Soe, K. Byth, C. H. Wong, Reduced complications from intracranial grid insertion by using a small grid size and a precise protocol during monitoring. *Acta Neurochir.* **158**, 395–403 (2016).
28. C. L. Stephan, J. J. Kepes, K. SantaCruz, S. B. Wilkinson, B. Fegley, I. Osorio, Spectrum of clinical and histopathologic responses to intracranial electrodes: From multifocal aseptic meningitis to multifocal hypersensitivity-type meningovasculitis. *Epilepsia* **42**, 895–901 (2001).
29. C. H. Wong, J. Birkett, K. Byth, M. Dexter, E. Somerville, D. Gill, R. Chaseling, M. Fearnside, A. Bleasel, Risk factors for complications during intracranial electrode recording in presurgical evaluation of drug resistant partial epilepsy. *Acta Neurochir.* **151**, 37–50 (2009).
30. T. Stieglitz, H. Beutel, M. Schuettler, J.-U. Meyer, Micromachined, polyimide-based devices for flexible neural interfaces. *Biomed. Microdevices* **2**, 283–294 (2000).
31. J. D. Yeager, D. J. Phillips, D. M. Rector, D. F. Bahr, Characterization of flexible ECoG electrode arrays for chronic recording in awake rats. *J. Neurosci. Methods* **173**, 279–285 (2008).
32. G. C. Wiggins, K. Elisevich, B. J. Smith, Morbidity and infection in combined subdural grid and strip electrode investigation for intractable epilepsy. *Epilepsy Res.* **37**, 73–80 (1999).
33. M. J. Nelson, P. Pouget, Do electrode properties create a problem in interpreting local field potential recordings? *J. Neurophysiol.* **103**, 2315–2317 (2010).
34. Y. Kajikawa, C. E. Schroeder, How local is the local field potential? *Neuron* **72**, 847–858 (2011).
35. E. W. Schomburg, C. A. Anastassiou, G. Buzsáki, C. Koch, The spiking component of oscillatory extracellular potentials in the rat hippocampus. *J. Neurosci.* **32**, 11798–11811 (2012).
36. C. A. Schevon, A. J. Trevelyan, C. E. Schroeder, R. R. Goodman, G. McKhann Jr., R. G. Emerson, Spatial characterization of interictal high frequency oscillations in epileptic neocortex. *Brain* **132** (Pt. 11), 3047–3059 (2009).
37. A. Hufnagel, M. Dümpelmann, J. Zentner, O. Schijns,C. E. Elger, Clinical relevance of quantified intracranial interictal spike activity in presurgical evaluation of epilepsy. *Epilepsia* **41**, 467–478 (2000).
38. C. Alvarado-Rojas, K. Lehongre, J. Bagdasaryan, A. Bragin, R. Staba, J. Engel Jr., V. Navarro, M. Le Van Quyen, Single-unit activities during epileptic discharges in the human hippocampal formation. *Front. Comput. Neurosci.* **7**, 140 (2013).
39. A. R. Wyler, G. A. Ojemann, A. A. Ward Jr., Neurons in human epileptic cortex: Correlation between unit and EEG activity. *Ann. Neurol.* **11**, 301–308 (1982).
40. A. C. Chamberlain, J. Viventi, J. A. Blanco, D.-H. Kim, J. A. Rogers, B. Litt, Millimeter-scale epileptiform spike patterns and their relationship to seizures. *Conf. Proc. IEEE Eng. Med. Biol. Soc.* **2011**, 761–764 (2011).
41. D. Khodagholy, J. Rivnay, M. Sessolo, M. Gurfinkel, P. Leleux, L. H. Jimison, E. Stavrinidou, T. Herve, S. Sanaur, R. M. Owens, G. G. Malliaras, High transconductance organic electrochemical transistors. *Nat. Commun.* **4**, 2133 (2013).

42. M. Sessolo, D. Khodagholy, J. Rivnay, F. Maddalena, M. Gleyzes, E. Steidl, B. Buisson, G. G. Malliaras, Easy-to-fabricate conducting polymer microelectrode arrays. *Adv. Mater.* **25**, 2135–2139 (2013).
43. D. Khodagholy, M. Gurfinkel, E. Stavrinidou, P. Leleux, T. Herve, S. Sanaur, G. G. Malliaras, High speed and high density organic electrochemical transistor arrays. *Appl. Phys. Lett.* **99**, 163304 (2011).

Acknowledgments: We thank V. Katlowitz (NYULMC) for intraoperative assistance. We thank M. Skvarla, R. Ilic, and M. Metzler from Cornell NanoScale Science and Technology Facility (CNF) for their technical support during device fabrication. We thank L. Melloni and P. Minhas for managing the IRB protocol of intraoperative epilepsy subject recordings at NYULMC. **Funding:** This work was supported by the NIH (grants NS 090583, MH54671, UO1NS099705, MH107396, and NS090526) and NSF Partnerships for International Research and Education: International Program for the Advancement of Neurotechnology. The device fabrication was performed at the CNF, a member of the National Nanotechnology Infrastructure Network, which is supported by the NSF (grant ECCS-0335765). D.K. is supported through the Simons Foundation (junior fellow). J.N.G. is supported by the Pediatric Scientist Development Program (March of Dimes). Z.Z. is supported by the China Scholarship Council. J.D.G. is supported by the NIH/National Institute on Deafness and Other Communication Disorders. **Author contributions:** D.K., J.N.G., G.B., and O.D. conceived the project. D.K., J.N.G., and Z.Z. designed, fabricated, and characterized the devices. D.K., J.N.G., and Z.Z. analyzed neural data. D.K. and J.N.G. did the intraoperative patient recordings. M.L. contributed to the intraoperative patient recordings. W.D. and J.D.G. were the attending neurosurgeons and conducted the intraoperative recordings. M.Y. did the intraoperative clinical electrophysiological recordings. W.D., J.D.G., and M.L. supervised the epilepsy patient recordings and IRB. J.N.G., D.K., and G.B. wrote the paper with input from the other authors. **Competing interests:** The authors declare that they have no competing interests. **Data and materials availability:** All data needed to evaluate the conclusions in the paper are present in the paper and/or the Supplementary Materials. Additional data related to this paper may be requested from the authors.

Submitted 7 May 2016
Accepted 7 October 2016
Published 9 November 2016
10.1126/sciadv.1601027

Citation: D. Khodagholy, J. N. Gelinas, Z. Zhao, M. Yeh, M. Long, J. D. Greenlee, W. Doyle, O. Devinsky, G. Buzsáki, Organic electronics for high-resolution electrocorticography of the human brain. *Sci. Adv.* **2**, e1601027 (2016).